

# Self-Supervised Learning with High-Stable Guidance Law and Label Generation for USV Trajectory Tracking Control

Shaowei Wang<sup>a</sup>, Wanneng Yu<sup>a,b,c,\*</sup>, Chuanbo Wu<sup>a</sup>, Haibin Wang<sup>d,\*</sup>, Longhai Xiao<sup>a,b</sup> and Yao Chen<sup>a,b,c</sup>

<sup>a</sup>*School of Marine Engineering, Jimei University, Xiamen 361021, PRC*

<sup>b</sup>*Fujian Provincial Key Laboratory of Naval Architecture and Ocean Engineering, Xiamen 361021, PRC*

<sup>c</sup>*Fujian Engineering and Research Center of Offshore Small Green Intelligent Ship System, Xiamen 361021, PRC*

<sup>d</sup>*Univ Strathclyde, Dept Naval Architecture Ocean & Marine Engn, Glasgow, Scotland*

## ARTICLE INFO

**Keywords:**

USV

Trajectory tracking

Guidance law

Label generation

Self-supervised learning

## ABSTRACT

Unmanned Surface Vehicle (USV) Systems confront significant challenges in achieving precise trajectory tracking, primarily attributed to their high coupling, nonlinear relationships, and external disturbances from environmental factors such as winds and currents. Addressing these obstacles is imperative for advancing the autonomy and performance of USVs. This paper introduces a self-supervised learning (SSL) based framework for USV trajectory tracking control. Firstly, we propose an adaptive look-ahead distance, which enhances the guidance law that exhibits remarkable stability, even at minimal look-ahead distances. Therefore, elevating the upper limit of guidance performance. Secondly, leveraging this refined guidance law, we develop a novel control label generation methodology specifically designed for USV trajectory tracking applications. This methodology facilitates the training of controllers via self-supervised learning, thereby circumventing the need for extensive and labor-intensive manual labeling processes. Finally, the proposed method is tested in multiple tracking scenarios, including simple and complex trajectories, and compared with the previous state-of-the-art (SOTA) approach. Simulation results demonstrate its effectiveness in achieving accurate trajectory tracking control for USVs.

## 1. Introduction

The Unmanned Surface Vehicle (USV) has become a critical focus of scientific and technological progress, paralleling advancements in unmanned aerial and ground vehicles. Its potential applications span diverse fields, including cargo transport, environmental surveillance, scientific exploration, and commercial operations, indicating substantial growth prospects (Dong et al., 2023; Yang et al., 2024). As a result, accurate trajectory tracking control (ATTC) for USVs is a fundamental objective in ocean engineering and control systems (Er et al., 2023). Nevertheless, semi-driven USVs present more complex control challenges than fully actuated systems, primarily due to restricted lateral control capabilities, where the number of controllable actuators is insufficient to match the vehicle's degrees of freedom. The mathematical models governing these USVs are characterized by pronounced nonlinearity and strong coupling, making their control highly vulnerable to environmental disturbances such as currents, waves, and winds (Yan et al., 2024), which significantly hinder ATTC performance. Therefore, developing robust and efficient control strategies for autonomous vessel systems is essential to achieve reliable trajectory tracking in dynamic and unpredictable environments, representing a persistent and unresolved challenge in this field.

Numerous control strategies have been developed to tackle the challenge of ATTC for USVs, encompassing techniques

such as feedback linearization, backstepping, nonlinear model predictive control, sliding mode control, neural networks, fuzzy logic, and adaptive control systems (Shin et al., 2017; Jia et al., 2019; Zhang et al., 2020; Deng et al., 2020; Liang et al., 2021). For instance, Chen et al. (2023) proposed an adaptive fixed-time backstepping control method tailored for 3D trajectory tracking of autonomous underwater vehicles (AUVs), addressing uncertainties in system models and external disturbances. Similarly, Zhao et al. (2021) introduced an advanced model predictive control framework that integrates a global course constraint and an event-triggered mechanism (ETM) to minimize deviations while optimizing energy efficiency. Meanwhile, Awad et al. (2022) designed a linear model predictive controller leveraging a Laguerre network and a fuzzy logic-based switching system to ensure accurate speed regulation and path tracking, accounting for input limitations and output noise. Certain approaches incorporate guidance laws to derive desired parameters, such as yaw angle and surge velocity, which are combined with controller inputs to achieve precise trajectory tracking. For example, Fan et al. (2023) developed a fixed-time sliding mode control (FTSMC) strategy incorporating a fixed-time extended state observer (FESO) and a fixed-time differentiator, utilizing saturation functions to prevent singularities. Additionally, Liu et al. (2023) presented a fixed-time robust control method based on the  $H_\infty$  technique to improve the performance and stability of unmanned underwater vehicles (UUVs), ensuring fast and accurate tracking, albeit with reliance on intricate parameter tuning and precise system modeling. On the other hand, Peng et al. (2021) adopted a data-

\*Corresponding authors:

 wnyu2007@jmu.edu.cn (Wanneng Yu); haibin.wang@strath.ac.uk

(Haibin Wang)

ORCID(s):

driven adaptive control approach, leveraging real-time data for model-free trajectory tracking, which enhances adaptability to unknown dynamics but demands significant computational power and high-quality data. Furthermore, Zhou et al. (2023) implemented an event-triggered approximate optimal path-tracking control scheme, reducing computational and communication overhead and making it suitable for resource-limited scenarios. However, it may exhibit instability in highly dynamic and uncertain environments, with approximate solutions not universally applicable. Recently, Wang et al. (2024) proposed a distributed prescribed-time formation control strategy for underactuated USVs, integrating neural networks for dynamic approximation and disturbance observers for error compensation while ensuring collision-free operation and connectivity maintenance through a prescribed-time tuning function and a novel nonlinear filter, significantly reducing the number of learning parameters and enhancing system performance.

Conventional control techniques, such as nonlinear model predictive control, fuzzy logic, and robust control, have been extensively applied in trajectory tracking applications, providing reliable and consistent performance under well-defined conditions. Nevertheless, these methods frequently rely on precise system models and face challenges in handling nonlinear behaviors and external perturbations. This results in notable performance declines when confronted with model inaccuracies and environmental fluctuations. Acknowledging these constraints highlights the need to investigate innovative strategies that deliver improved adaptability and robustness in dynamic and uncertain scenarios.

The rapid evolution of artificial intelligence (AI) has boosted the widespread integration of machine learning techniques into diverse fields, especially in the realm of control systems (Xiaofei et al., 2022; Wu et al., 2023; Li et al., 2025). In the context of USVs, significant research efforts have been directed toward leveraging AI for enhanced control capabilities. For instance, Wang et al. (2022) developed an actor-critic-based finite-time reinforcement learning framework to achieve accurate USV trajectory tracking under unknown system dynamics and input limitations. This guarantees that tracking errors converge to a predefined precision within a finite time. Similarly, Wang et al. (2021) tackled complex uncertainties, such as dead zone nonlinearities, by formulating an optimal tracking control strategy using reinforcement learning. However, it encountered issues with limited input data and slow online adaptation. Meanwhile, Zhang et al. (2022) proposed a hybrid control method combining model-referenced techniques with reinforcement learning, which improved control performance but lacked efficiency in data sampling and failed to address environmental disturbances adequately. Additionally, Woo et al. (2019) demonstrated a robust tracking control method by integrating vector field guidance with deep deterministic policy gradient (DDPG) algorithms, showcasing its effectiveness in diverse experimental settings for full-scale USVs. In a recent study, Liu et al. (2024) proposed an event-triggered optimal tracking control method for underactuated USVs using

a neural reinforcement learning approach, which stabilizes tracking errors within an asymmetric prescribed-time range, eliminates initial condition limitations, and reduces communication and actuator execution burdens through a relative threshold event-triggered mechanism. More recently, Wu et al. (2024) introduced an advanced deep reinforcement learning framework incorporating an intrinsic curiosity module (ICM) within a proximal policy optimization (PPO) structure, effectively managing system complexities and external disturbances. Furthermore, Peng et al. (2024) proposed an online deep learning control strategy that utilizes deep neural networks (DNNs) for real-time dynamic modeling and an extended state observer (ESO) to estimate and mitigate modeling inaccuracies, significantly improving trajectory tracking performance in varying maritime conditions.

Supervised learning (SL) and deep reinforcement learning (DRL) encounter challenges related to labeled data dependency or sample inefficiency. Self-supervised learning (SSL), which has been highlighted in recent research (Gui et al., 2024; Abdulrazzaq et al., 2024), offers a promising solution by leveraging data collected without manual labeling to learn discriminative features, thereby minimizing the reliance on labeled datasets and demonstrating significant advancements in various fields. For instance, Ginerica et al. (2021) proposed a vision-dynamics learning approach, ObserveNet Control, for autonomous vehicles, which predicts future sensory data and computes safe trajectories in a self-supervised manner, demonstrating its effectiveness in aggressive driving scenarios without the need for manual labeling. Similarly, Chu et al. (2024) introduced a self-supervised dock pose estimator (SDPE) for USVs, enabling autonomous docking through a monocular camera-based pipeline that eliminates manual labeling and camera calibration, achieving precise position-based visual servoing in simulated environments. Another compelling application of SSL is in the intuitive control systems, such as sonomyography-based prosthetic hand control (Yang et al., 2025), highlighting its suitability for tasks demanding high precision and adaptability. Against these backdrops, integrating SSL into trajectory tracking control for USVs presents a compelling research direction. This paper introduces a novel SSL-based trajectory tracking control framework to enhance USV performance through an optimized guidance law and a tailored label generation mechanism. The key contributions of this work are outlined as follows:

(1) Adaptive Look-Ahead Distance Algorithm: We introduce an innovative adaptive look-ahead distance algorithm to augment the guidance law. This algorithm demonstrates exceptional stability, even at minimal look-ahead distances, thereby significantly elevating the upper limit of guidance performance and enhancing the overall precision of trajectory tracking for USVs.

(2) Automated Control Label Generation: Leveraging the refined guidance law, we propose a novel control label generation method tailored for USV trajectory tracking tasks. This method automates the process of generating control labels required for training, drastically reducing the dependency on

labor-intensive manual labeling and accelerating the development of efficient controllers.

(3)Comprehensive Simulation Tests: To validate the effectiveness and superiority of our method, we conduct extensive simulation tests across a diverse range of trajectory-tracking scenarios, including both simple and complex paths. The results unequivocally demonstrate the robustness and accuracy of our approach in achieving precise trajectory tracking for USVs, underpinning its potential for real-world applications.

## 2. Problem statement

This section outlines the kinematic and dynamic models of a USV equipped with a single propeller and rudder. The system's control inputs are defined as the propeller revolution and the rudder angle, which collectively facilitate the USV's ability to follow a reference path.

### 2.1. USV dynamic model

USV motion control encompasses six degrees of freedom. In order to balance computational efficiency and model accuracy, this study employs a simplified three-degree-of-freedom maneuvering model for trajectory tracking control, as described in Yasukawa and Yoshimura (2015).

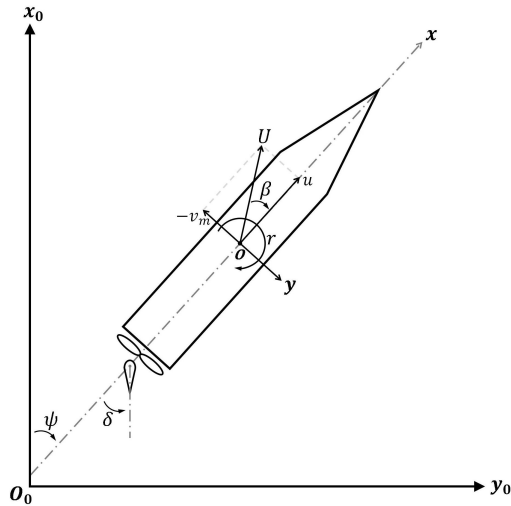


Fig. 1. Coordinate systems of USV motion.

As illustrated in Fig. 1, two coordinate systems are employed: the space-fixed coordinate system  $O_o - x_o y_o$ , with the  $x_o - y_o$  plane parallel to the horizontal, and the moving ship-fixed coordinate system  $O - xy$ , centered at midship, where  $O_x$  points to the bow and  $O_y$  to the starboard. The heading angle  $\psi$  is the angle between  $O_o x_o$  and  $Ox$ . Velocity components along  $x$  and  $y$ , and yaw rate are denoted by  $u$ ,  $v_m$ , and  $r$ , respectively. The rudder angle is  $\delta$ , drift angle  $\beta = \tan^{-1}(-v_m/u)$ , and combined velocity  $U = \sqrt{u^2 + v_m^2}$ . The USV's center of gravity  $G$  is at  $(x_G, 0)$  in  $O - xy$ , with lateral velocity at  $G$  given by  $v = v_m + x_G r$ .

The kinematic model is described by Eq. (1):

$$\begin{bmatrix} \dot{x} \\ \dot{y} \\ \dot{\psi} \end{bmatrix} = \begin{bmatrix} \sin(\psi) & \cos(\psi) & 0 \\ -\cos(\psi) & \sin(\psi) & 0 \\ 0 & 0 & 1 \end{bmatrix} \begin{bmatrix} u \\ v_m \\ r \end{bmatrix} \quad (1)$$

The dynamics model is described by Eq. (2):

$$\begin{cases} (m + m_x)\dot{u} - (m + m_y)v_m r = X \\ (m + m_y)\dot{v}_m - (m + m_x)ur = Y \\ (I_{ZZ} + J_{ZZ})\dot{r} + x_G m(\dot{v}_m + ur) = N_m \end{cases} \quad (2)$$

where  $m$  represents the ship's mass,  $m_x$  and  $m_y$  denote additional masses along the  $x$  and  $y$  axes, respectively.  $x_G$  is the longitudinal center of gravity coordinate of the USV.  $I_{ZZ}$  is the moment of inertia around the center of gravity, with  $J_{ZZ}$  as the added moment of inertia.  $X$ ,  $Y$ , and  $N_m$  signify the longitudinal force, transverse force, and transverse moment, respectively. These expressions are derived based on the motion and force characteristics of the USV with a single propeller and rudder, as shown in Eq. (3):

$$\begin{cases} X = X_H + X_P + X_R + X_{wind} + X_{wave} \\ Y = Y_H + Y_R + Y_{wind} + Y_{wave} \\ N_m = N_H + N_R + N_{wind} + N_{wave} \end{cases} \quad (3)$$

where subscripts H, P, and R denote hull, propeller, and rudder, respectively, while wind and wave denote environmental disturbances during navigation. Refer to Wu et al. (2024) for more details.

### 2.2. Problem formulation

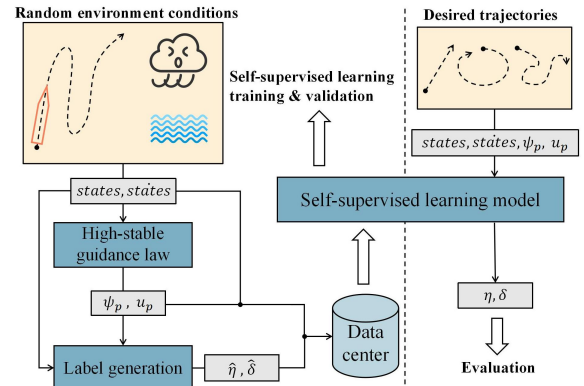
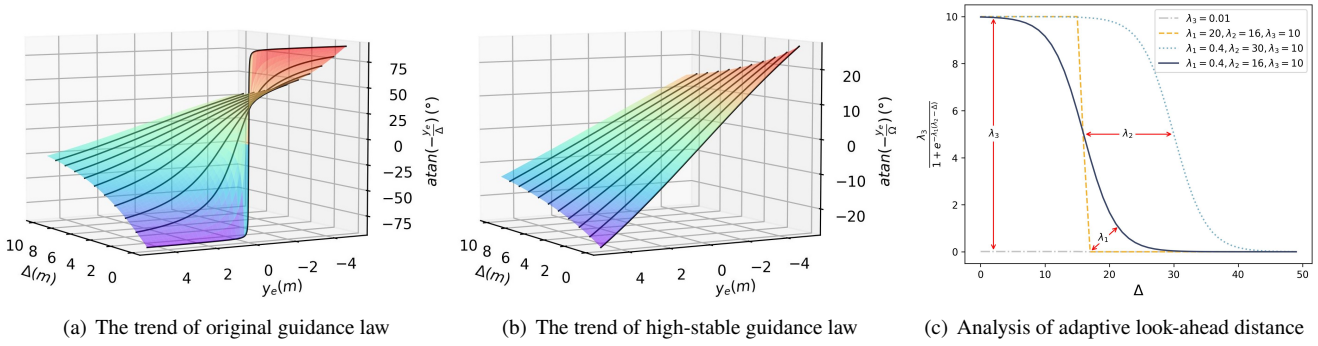


Fig. 2. Overall control Architecture.

Within the realm of USV control, automatic trajectory tracking faces notable challenges. Our research endeavor focuses on devising a controller capable of precisely and stably following a predefined smooth path, where the bounded derivatives of this trajectory bolster the controller's stability and operational efficiency. This controller evaluates the current state of the USV and computes a tracking error, denoted as  $\|p(t) - p_d(t)\|$ , which quantifies the deviation from



**Fig. 3.** The evolution process of guidance law.

the reference path. A self-supervised learning-based controller (SSL) is introduced in this study. The research proposes an improved high-stable guidance law with adaptive look-ahead distance, followed by a control label generation technique specifically designed for USV trajectory tracking. The SSL model is trained on data collected from randomly generated environmental conditions, guidance law, and label generation. It is then tested across various tracking scenarios, demonstrating its effectiveness in achieving accurate USV trajectory tracking. The comprehensive control system architecture is depicted in Fig. 2. Additional insights into the guidance law, label generation, and experimental evaluations are provided in Sections 3, 4, and 5, respectively.

### 3. High-stable guidance law

Based on the guidance law described in the literature (Huang et al., 2019; Wu et al., 2024), the along-track error  $x_e$ , the cross-track error  $y_e$ , their time derivatives  $\dot{x}_e$  and  $\dot{y}_e$ , as well as the desired heading angle  $\psi_p$  and surge  $u_p$  can be defined according to Equations (4), (5), and (6), respectively.

$$\begin{bmatrix} x_e \\ y_e \end{bmatrix} = \begin{bmatrix} \cos(\psi_d) & \sin(\psi_d) \\ -\sin(\psi_d) & \cos(\psi_d) \end{bmatrix} \begin{bmatrix} x - x_d(t) \\ y - y_d(t) \end{bmatrix} \quad (4)$$

$$\begin{cases} \dot{x}_e = U \cos(\psi - \psi_d + \beta) - U_d + y_e \dot{\psi}_d \\ \dot{y}_e = U \sin(\psi - \psi_d + \beta) - x_e \dot{\psi}_d \end{cases} \quad (5)$$

$$\begin{cases} \psi_p = \psi_d + \text{atan}\left(-\frac{y_e}{\Delta}\right) - \beta \\ u_p = \sqrt{U_p^2 - v^2} \\ U_p = \frac{(U_d - kx_e)\sqrt{y_e^2 + \Delta^2}}{\Delta} \end{cases} \quad (6)$$

Where  $\psi_d(\omega) = \text{atan2}(y'_d(t), x'_d(t)) \in [-\pi, \pi]$  denotes the tangent angle of the trajectory.  $U = \sqrt{u^2 + v^2}$ ,  $\beta = \text{atan2}(v, u)$  and  $U_d = \sqrt{\dot{x}_d^2 + \dot{y}_d^2}$ . While  $\Delta > 0$  is the look-ahead distance and  $k > 0$  is the controller gain.

This paper builds upon the guidance law shown in the Eq. (6), and enhances it by introducing an adaptive look-ahead distance. In Eq. (6), the term  $\text{atan}\left(-\frac{y_e}{\Delta}\right)$  represents the corrective response to the cross-track distance, enabling the USV to converge upon the reference path. As illustrated in Fig. 3(a), due to  $\lim_{\Delta \rightarrow 0^+, y_e \neq 0} \text{atan}\left(-\frac{y_e}{\Delta}\right) = \pm \frac{\pi}{2}$ , when the look-ahead distance  $\Delta$  approaches smaller values, the guidance law generates extremely large heading angle candidates. While this can be acceptable when the cross-track distance is substantial, it becomes problematic when minimal, as the rudder angles fluctuate significantly. Such fluctuations are detrimental for maintaining a stable heading and degrade guidance performance. In order to address this issue, we proposed an adaptive look-ahead distance mechanism, as detailed below, to enhance the guidance performance:

$$\Delta \in \left\{ \Omega = \Delta + \frac{\lambda_3}{1 + e^{-\lambda_1(\lambda_2 - \Delta)}} \right\} \quad (7)$$

where  $\lambda_1 > 0$ ,  $\lambda_2 > 0$ , and  $\lambda_3 > 0$  are the hyperparameters of the adaptive look-ahead distance. As shown in Fig. 3(c), when  $\lambda_3 = 0.01$ ,  $\Delta \approx \Omega$ , implying that  $\Delta \in \Omega$ . When  $\lambda_1$  assumes a large value, the numerical trend closely resembles a piecewise function. Conversely, smaller values of  $\lambda_1$  result in a smoother variation. Furthermore,  $\lambda_2$  delineates between employing the adaptive look-ahead distance and retaining the original guidance responsiveness. In our experimental setup, the specific hyperparameters utilized were  $\lambda_1 = 0.82$ ,  $\lambda_2 = 16.08$ , and  $\lambda_3 = 10.01$ . The methodology for searching and determining these hyperparameters will be detailed in Section 5.1. The refined high-stable guidance law is formally defined as follows:

$$\begin{cases} \psi_p = \psi_d + \text{atan}\left(-\frac{y_e}{\Omega}\right) - \beta \\ u_p = \sqrt{U_p^2 - v^2} \\ U_p = \frac{(U_d - kx_e)\sqrt{y_e^2 + \Omega^2}}{\Omega} \end{cases} \quad (8)$$

Based on the relationship  $\Delta \in \Omega$ , it can be deduced that Eq. (6)  $\in$  Eq. (8), thereby suggesting that the high-stable guidance law constitutes a superset of the original guidance

law. As illustrated in Fig. 3(b), the high-stable guidance law balances responsiveness and stability across various look-ahead distances. The following section will continue to demonstrate the stability of this refined guidance law.

Furthermore, If the following error signals  $E_\psi$  and  $E_u$  can converge to zero, the convergence of the position error is guaranteed.

$$\begin{cases} E_\psi = \psi - \psi_p \\ E_u = u - u_p \end{cases} \quad (9)$$

Proof consider the following Lyapunov function candidate:

$$V_1 = \frac{1}{2}x_e^2 + \frac{1}{2}y_e^2 \quad (10)$$

Differentiating Eq. (10), and substituting Eq. (5) into it, yields:

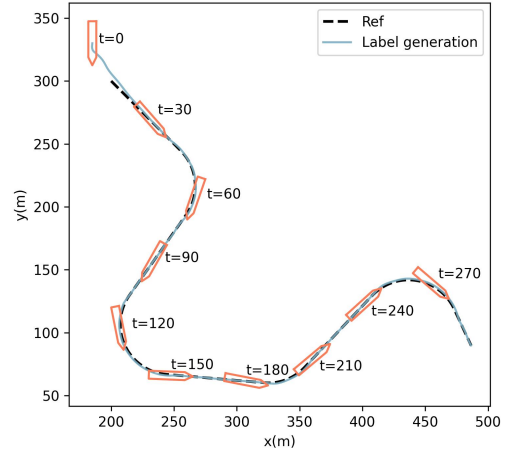
$$\begin{aligned} \dot{V}_1 &= x_e \dot{x}_e + y_e \dot{y}_e \\ &= x_e [U \cos(\psi - \psi_d + \beta) - U_d + y_e \dot{\psi}_d] \\ &\quad + y_e [U \sin(\psi - \psi_d + \beta) - x_e \dot{\psi}_d] \\ &= x_e U \cos \left[ \text{atan} \left( -\frac{y_e}{\Omega} \right) \right] - x_e U_d \\ &\quad + y_e U \sin \left[ \text{atan} \left( -\frac{y_e}{\Omega} \right) \right] \\ &= x_e \left[ \frac{(U_d - kx_e) \sqrt{y_e^2 + \Omega^2}}{\Omega} \right] \frac{\Omega}{\sqrt{y_e^2 + \Omega^2}} - x_e U_d \\ &\quad + y_e \left[ \frac{(U_d - kx_e) \sqrt{y_e^2 + \Omega^2}}{\Omega} \right] \frac{-y_e}{\sqrt{y_e^2 + \Omega^2}} \\ &= -kx_e^2 - \frac{y_e^2}{\Omega} (U_d - kx_e) \\ &= -kx_e^2 - \frac{y_e^2}{\Omega} \left( \frac{U\Omega}{\sqrt{y_e^2 + \Omega^2}} + kx_e - kx_e \right) \\ &= -kx_e^2 - \frac{Uy_e^2}{\sqrt{y_e^2 + \Omega^2}} \end{aligned} \quad (11)$$

Given that  $k$  is positive, it is evident that the derivative of  $V_1$ , denoted as  $\dot{V}_1$ , is non-positive. Consequently, it is logical to deduce that  $x_e$  and  $y_e$  tend towards zero.

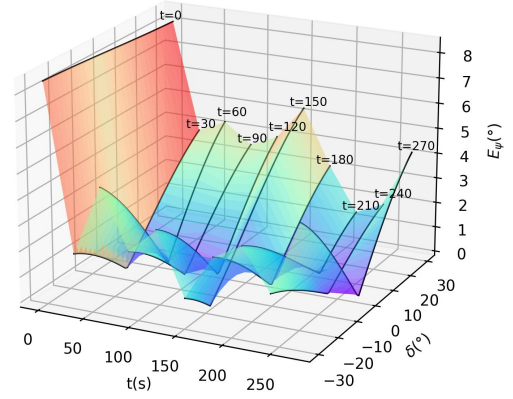
#### 4. Label generation and SSL-based controller

In this section, we introduce a novel label generation approach for control values, which is grounded in an in-depth analysis of the interplay between control values and guidance values. Subsequently, leveraging the high-stable guidance law and the control labels generated, a self-supervised learning-based controller is designed.

#### 4.1. Guidance law-based label generation



(a) Tracking the complex trajectory



(b) The trend of signal errors

**Fig. 4.** Relationship between rudder angle and signal error.

According to Eq. (9) of the high-stable guidance law, the signal errors of control values can be formulated as follows:

$$\begin{cases} E_\psi(\eta_i, \delta_i) = \psi(\eta_i, \delta_i) - \psi_p \\ E_u(\eta_i, \delta_i) = u(\eta_i, \delta_i) - u_p \end{cases} \quad (12)$$

where  $\eta_i \in \eta = \{0, 1, 2, \dots, \eta_{max}\}$  denotes the discrete propeller revolution, while the discrete rudder angle is represented as  $\delta_i \in \delta = \{\delta_{min}, \delta_{min} + 1, \delta_{min} + 2, \dots, \delta_{max}\}$ . Fig. 4 elucidates the correlation between rudder angle and signal error in the complex path detailed in the experimental section 5.3.3. Specifically, Fig. 4(a) demonstrates the USV utilizes the generated control label to track complex trajectories. Whereas Fig. 4(b) portrays the relationship between the rudder angle, signal error, and time change. It is evident that across various time intervals, the signal error exhibits either a single extremum or a monotonic trend, where the extremum occurs at the boundary of the control value range. Consequently, the extremum point can be intuitively deemed the optimal control variable. Hence, the methodology for generating control labels can be expressed as follows:

$$\begin{cases} \hat{\eta}^t = \operatorname{argmin}_i [E_u(\eta_i^t, \hat{\delta}^{t-1})] \\ \hat{\delta}^t = \operatorname{argmin}_i [E_\psi(\hat{\eta}^t, \delta_i^t)] \end{cases} \quad (13)$$

where  $\hat{\eta}^t$  and  $\hat{\delta}^t$  represent the ground truth of propeller revolution and rudder angle, respectively. Among them, when acquiring the control label for the propeller revolution, denoted as  $\hat{\eta}^t$ , we employ the previously recorded ground truth of the rudder angle,  $\hat{\delta}^{t-1}$ , as an approximating estimate.

## 4.2. Self-supervised learning-based controller

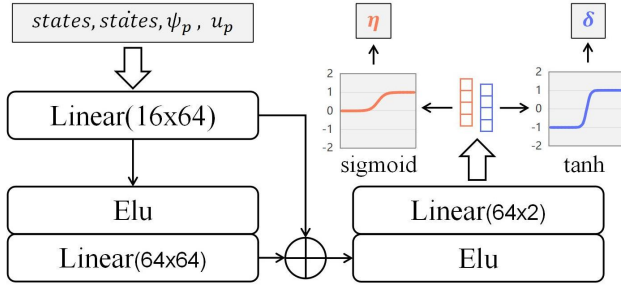


Fig. 5. Overall architecture of SSL model.

In the design of our self-supervised learning-based controller (SSL) for USVs, the input features are selected according to the approach outlined in Wu et al. (2024). The input vector  $S$  comprises the current state of the USV, including its position, velocity, the deviation between the control value and the guidance value, and the temporal derivatives of these states. It comprehensively represents the vessel's operational status, empowering the neural network to learn the intricate relationships between the control values and the resulting trajectory. The choice of these inputs is crucial as they directly influence the controller's ability to adapt to various operational scenarios and environmental disturbances.

$$S \in \{x_e, y_e, \Delta_\psi, \Delta_u, u, v, r, \dot{x}_e, \dot{y}_e, \dot{\Delta}_\psi, \dot{\Delta}_u, \dot{u}, \dot{v}, \dot{r}, \eta, \delta\} \quad (14)$$

The output layer of our SSL controller is responsible for generating precise trajectory-tracking control commands. It specifically predicts propeller revolution and rudder angle, the key actuators for USV motion control. As shown in Fig. 5, we employ tanh or sigmoid activation functions for output scaling to constrain predictions within physically feasible ranges. Consequently, the output action  $A$  is formulated as Eq. (15).

$$A = \{\eta, \delta\} \quad (15)$$

Fig. 5 depicts the overall architecture of our SSL controller, a deep self-supervised learning model  $A = SSL(S)$  tailored for efficient state-to-control mapping. The network's representation layer comprises two linear layers, each followed by an ELU (Exponential Linear Unit) activation to

introduce nonlinearity and bolster representational capacity. Residual connections between these layers enhance learning efficiency and convergence by facilitating gradient flow during backpropagation. The input layer receives state and derivative data, and the final output layer applies tanh or sigmoid to the features of the control values, yielding scaled propeller revolution and rudder angle. This design ensures the controller captures USV dynamics accurately, generating precise control actions while maintaining lightweight parameters.

An appropriate loss function is essential for quantifying the discrepancy between the predicted and desired control values in training our SSL controller. In this work, we utilize the smooth L1 loss function, which combines the benefits of L1 and L2 losses. It is less sensitive to outliers than L2 loss and offers smoother gradients near zero errors than L1 loss. The loss function is defined as:

$$\begin{cases} loss = \text{smooth}_{L1}(\eta - \hat{\eta}) + \text{smooth}_{L1}(\delta - \hat{\delta}) \\ \text{smooth}_{L1}(x) = \begin{cases} 0.5x^2 & \text{if } |x| < 1 \\ |x| - 0.5 & \text{otherwise} \end{cases} \end{cases} \quad (16)$$

where  $x$  represents the difference between the predicted and target control values, by minimizing this loss function during training, our SSL controller learns to produce control values that closely match the desired trajectory, thereby enhancing the overall tracking performance of the USV.

## 5. Experiments

In this chapter, we conduct a comprehensive set of experiments to validate the effectiveness and robustness of our method. These experiments are designed to rigorously test the proposed methodology under various tracking scenarios, ranging from simple to complex trajectories. By evaluating performance metrics such as tracking accuracy, stability, and adaptation to environmental disturbances, we aim to demonstrate the superiority of our approach. This chapter presents the details of the hyperparameter search process, the self-supervised learning (SSL) training procedure, and the comprehensive simulation results obtained for different tracking tasks.

### 5.1. Hyperparameter search

This section details the hyperparameter search for Eq. (7), involving  $\lambda_1$ ,  $\lambda_2$ , and  $\lambda_3$ . Various hyperparameter combinations were tested in the complex trajectory outlined in Section 5.3.3, using labels generated as control values to minimize tracking errors. Fig. 6 presents the search results, comprising four subplots that depict the optimization process. Fig. 6(a) shows a 3D plot with axes for  $\lambda_1$  (0 to 20, step by 1),  $\lambda_2$  (0 to 20, step by 1), and  $\lambda_3$  (0 to 40, step by 1). Gray points represent the top 10% combinations with lower errors, while yellow points indicate the bottom 10% with higher errors. The optimal combination ( $\lambda_1 = 1$ ,  $\lambda_2 = 17$ ,  $\lambda_3 = 10$ ) is marked by a red triangle. Notably, poor combinations cluster

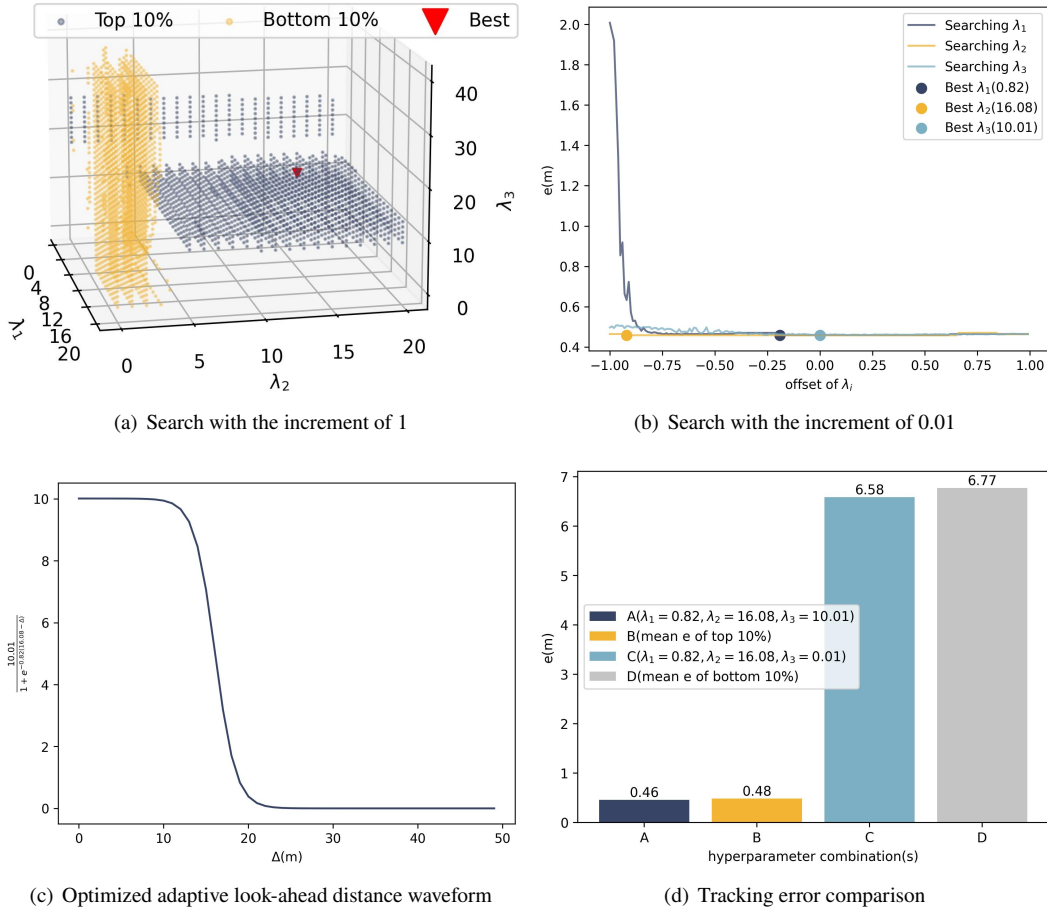


**Fig. 6.** Hyperparameter search.

around low  $\lambda_2$  values (0-5), whereas optimal combinations predominantly lie in the region where  $\lambda_1 < 16$ ,  $\lambda_2 > 5$ , and  $\lambda_3 > 7$ . This distribution highlights the importance of the adaptive look-ahead distance for high-stable guidance law.

Building upon the insights gained from Fig. 6(a), Fig. 6(b) delves into a finer-grained search by fixing two of the hyperparameters and varying the third with an increment of 0.01. This analysis reveals that variations of  $\lambda_1$  have a more pronounced impact on the tracking error compared to  $\lambda_2$  and  $\lambda_3$ . Finally, the refined hyperparameters determined at a precision of 0.01 are  $\lambda_1 = 0.82$ ,  $\lambda_2 = 16.08$ , and  $\lambda_3 = 10.01$ . These values offer a balance that minimizes the tracking error. Fig. 6(c) displays the waveform of the adaptive look-ahead distance function using the optimized hyperparameters. The waveform exhibits a smooth transition rather than being close to zero or a piecewise function, indicating the necessity to employ the adaptive look-ahead distance to achieve high-stable guidance performance. Finally, Fig. 6(d) presents a bar chart comparing the tracking errors. Bar A represents the mean error with the optimal hyperparameter combination (0.46), Bar B shows the mean error for the top 10% (0.48), Bar C indicates the mean error without optimization (6.58) where  $\lambda_3=0.01$ , and Bar D denotes the mean error for the bottom 10% (6.77). These comparisons further

demonstrate the importance of a high-stable guidance law to enhance the overall performance of the USV trajectory tracking control.

## 5.2. SSL training

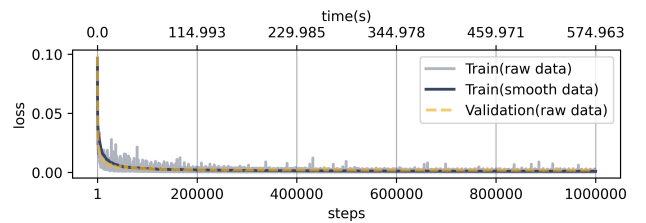


**Fig. 7.** Learning curves of SSL model.

In the SSL training phase, we employed a dataset comprising randomly generated environmental conditions and the corresponding control labels generated by our proposed label generation technique. The dataset was divided into a 90% training set and a 10% validation set. The random factors included the angles and lengths for straight paths, the initial angles, central angles, and clockwise/counterclockwise directions for circular paths, the initial heading angles and positions of the vessel, as well as the random wind directions

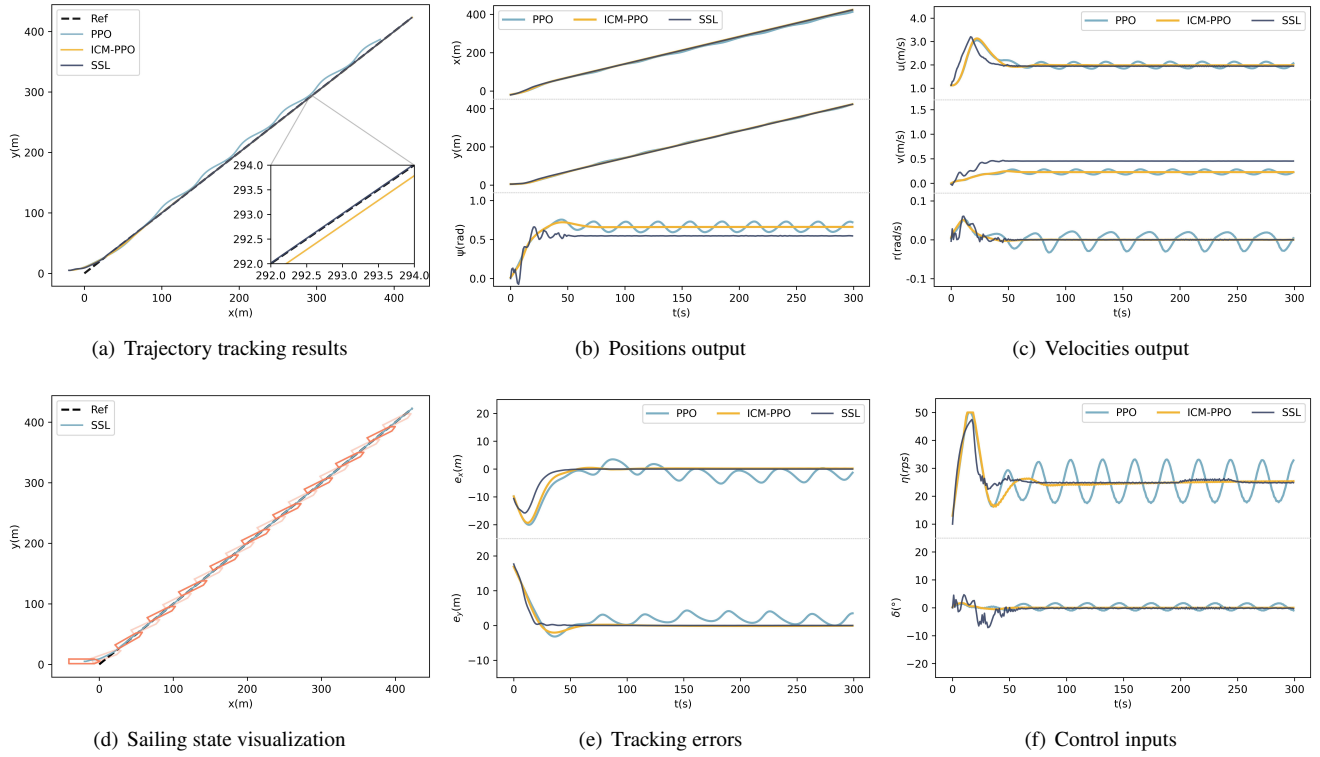


**Fig. 8.** Straight trajectory tracking performance.

and speeds and random current directions and velocities. Input saturation limits were imposed, with propeller revolution ranging from 0 to 50 RPS and rudder angle between -30 and 30 degrees. A total of 88,218 data samples were collected in random environments based on the SSL model's input-output configuration, and the model was trained for 1 million iterations, utilizing the best-performing model on the validation set for testing straight, circular, and complex trajectories. The hyperparameters used during training were a batch size of 256, a learning rate of 0.001, and the Adam optimizer.

The SSL training was conducted on a high-performance experimental setup featuring a 13th Gen Intel i7-13700 CPU with 24 threads, DDR4 3200MHz memory, and a Tesla T4 GPU running on Ubuntu 24.04 LTS. As shown in the learning curves in Fig. 7, both training and testing phases demonstrate rapid convergence within a short time. Even during prolonged training sessions to identify the best validation model, the process maintains consistent stability. When configured with the batch size of 256, the computational throughput maintains sub-millisecond latency per batch, exceeding the rigorous benchmarks for real-time processing requirements. Compared to deep reinforcement learning, our approach achieves higher data efficiency and eliminates the need for additional random exploration. The training sampling rate is 1/100, while the testing sampling rate is 1/1000, ensuring an efficient and balanced evaluation process. This robust performance underscores the effectiveness and practicality of our SSL training methodology.

**Table 1**

Error analysis of straight trajectory tracking experiments.

Method	Mean value of $e_x$ after 50 s	Mean value of $e_y$ after 50 s	Mean value of $e$ after 50 s
PPO	1.952m	1.829m	2.954m
ICM-PPO	0.202m	0.136m	0.254m
SSL	<b>0.018m</b>	<b>0.007m</b>	<b>0.020m</b>

### 5.3. Simulation results

The 7 m long and 1.16 m wide KVLCC2 cruise ship model was the target vessel for simulation experiments, with relevant hydrodynamic parameters detailed in Yasukawa and Yoshimura (2015). As performed in the ICM-PPO paper (Wu et al., 2024), the tracking control effects of PPO, ICM-PPO, and SSL are comparatively analyzed across various scenarios to verify the effectiveness and robustness of our method (SSL).

#### 5.3.1. Straight trajectory

$$\begin{cases} x_d(t) = \sqrt{2}t \\ y_d(t) = \sqrt{2}t \end{cases} \quad (17)$$

In the straight-line trajectory tracking simulation, the initial conditions were set as follows: the position and heading angle were  $\{x_0 = -20 \text{ m}, y_0 = 5 \text{ m}, \psi_0 = \frac{4}{3}\pi\}$ , and the initial velocities were  $\{u_0 = 1.128 \text{ m/s}, v_0 = 0 \text{ m/s}, r_0 =$

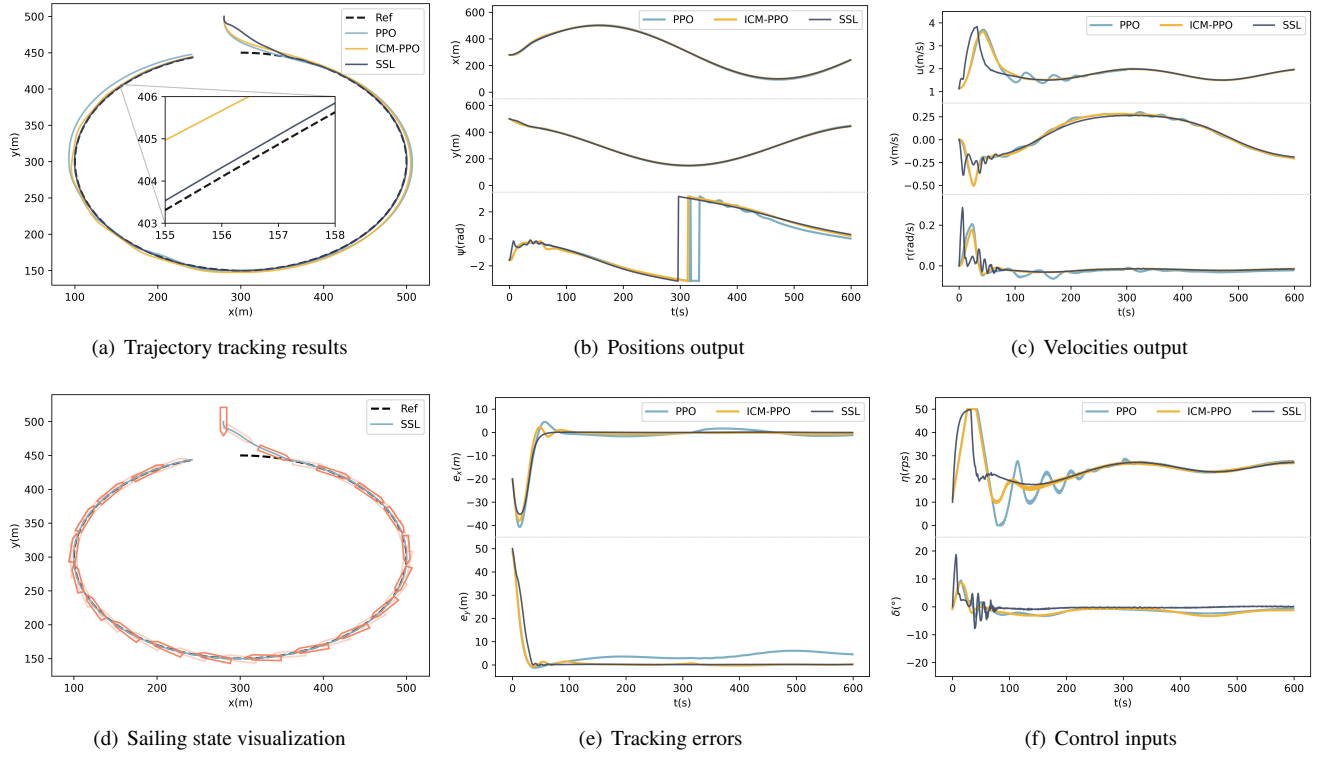


**Fig. 9.** Circular trajectory tracking performance.

$0 \text{ rad/s}$ . The control parameters were initialized at  $\eta_0 = 10 \text{ r/s}$  and  $\delta_0 = 0^\circ$ . Environmental factors included a southeast (SE,  $135^\circ$ ) wind with a speed of  $3 \text{ m/s}$  and a southeast (SE,  $135^\circ$ ) current with a velocity of  $0.5 \text{ m/s}$ .

The USV's straight-line trajectory tracking simulation outcomes are depicted in Fig. 8, illustrating the comparative tracking efficacy among the PPO, ICM-PPO, and SSL methodologies. As evidenced by Fig. 8(a) to Fig. 8(d), each approach demonstrates the capacity to adhere to the reference path despite disruptive influences. After the 50-second mark, the PPO method began to display deviations attributable to the forces of southeast winds and currents. In contrast, the ICM-PPO and SSL methodologies sustained precise trajectory adherence under identical environmental challenges. Particularly, the SSL approach demonstrated superior control accuracy within the proximal visual range. Analysis of the heading alteration graph reveals a stabilization in the heading angle's fluctuation magnitude beyond the 50-second interval. Following this, the SSL method consistently upheld a steady heading, facilitating exact tracking. The heading angle settled at  $0.491 \text{ rad}$ , diverging from the target of  $0.785 \text{ rad}$ , yet it proficiently mitigated the disturbances caused by winds and currents. Regarding velocity tracking, the refined method showcased commendable stability relative to its counterparts, with velocity variations equilibrating after 60 seconds. Consequently, the SSL technique surpasses the PPO and ICM-PPO methods in enhancing tracking precision across positional, heading, and velocity dimensions.

**Table 2**

Error analysis of circular trajectory tracking experiments.

Method	Mean value of $e_x$ after 50 s	Mean value of $e_y$ after 50 s	Mean value of $e$ after 50 s
PPO	1.895m	3.674m	3.987m
ICM-PPO	0.517m	0.269m	0.646m
SSL	<b>0.077m</b>	<b>0.189m</b>	<b>0.218m</b>

The trajectory errors across methodologies are presented in Fig. 8(e). Comparative analysis reveals that the SSL approach accelerates error convergence during trajectory tracking. Upon stabilization of the USV's linear path, the mean tracking error for SSL measures  $0.02 \text{ m}$ , representing reductions of  $2.934 \text{ m}$  and  $0.234 \text{ m}$  relative to PPO and ICM-PPO methods, respectively, as quantified in Table 1. Examination of the control input profiles in Fig. 8(f) demonstrates SSL's rapid response to initial large-scale deviations. The algorithm optimizes control inputs to mitigate positional offsets and environmental perturbations, achieving enhanced tracking precision. Notably, this adaptive compensation mechanism contributes to SSL's superior performance in maintaining trajectory accuracy under dynamic disturbances.

### 5.3.2. Circular trajectory

$$\begin{cases} x_d(t) = 200 \sin(0.01t) + 300 \\ y_d(t) = 150 \cos(0.01t) + 300 \end{cases} \quad (18)$$

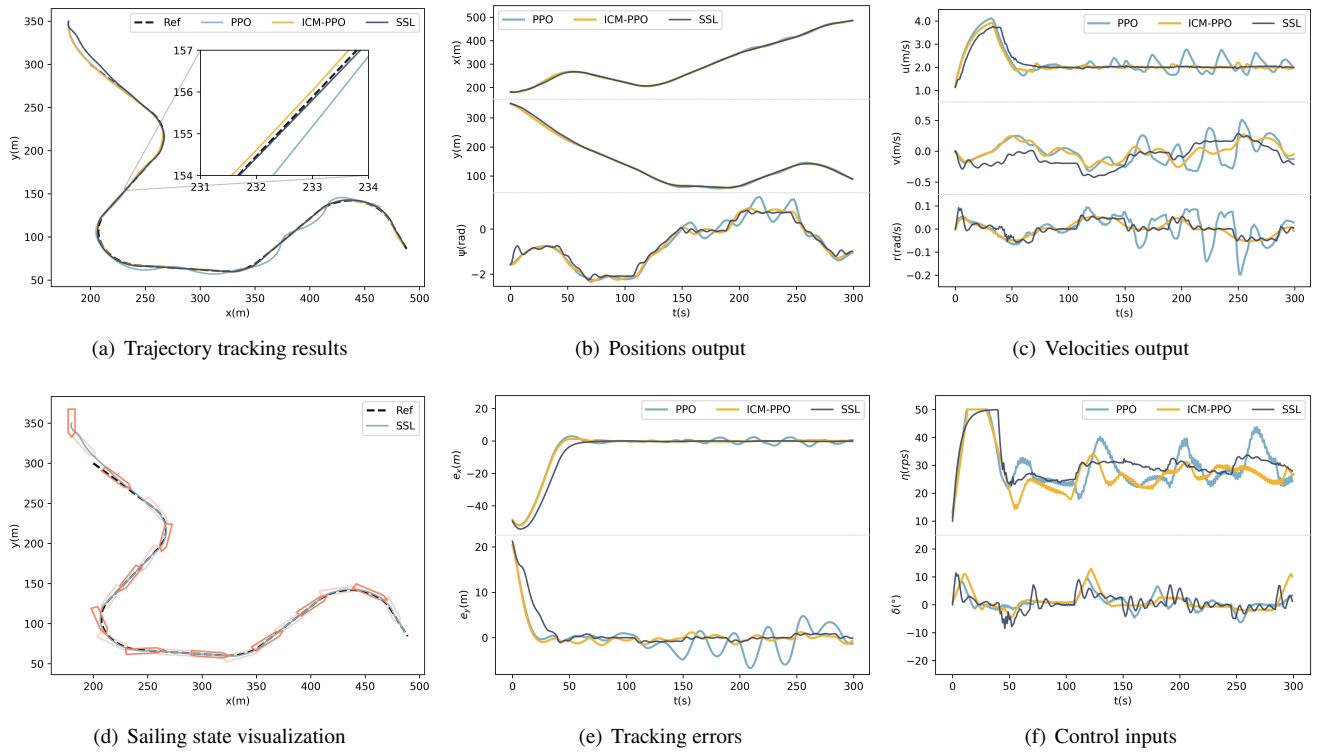


**Fig. 10.** Complex trajectory tracking performance.

In the circular trajectory tracking simulation, the initial conditions were set as follows: the position and heading angle were  $\{x_0 = 280\text{ m}, y_0 = 500\text{ m}, \psi_0 = \frac{2}{3}\pi\}$ , and the initial velocities were  $\{u_0 = 1.128\text{ m/s}, v_0 = 0\text{ m/s}, r_0 = 0\text{ rad/s}\}$ . The control parameters were initialized at  $\eta_0 = 10\text{ r/s}$  and  $\delta_0 = 0^\circ$ . Environmental factors included a east (E,  $90^\circ$ ) wind with a speed of  $3\text{ m/s}$  and a east (E,  $90^\circ$ ) current with a velocity of  $0.25\text{ m/s}$ .

The comparative analysis of circular trajectory tracking performance is depicted in Fig. 9, where Fig. 9(a) to Fig. 9(d) demonstrate that all evaluated methods successfully follow the reference path under interference conditions. Specifically, Fig. 9(a) highlights that PPO experiences notable deviations between 80-200 s and 350-600 s due to eastward environmental forces, whereas ICM-PPO and SSL maintain satisfactory tracking accuracy. SSL exhibits superior precision and dynamic responsiveness across the entire duration. The heading change analysis indicates that both heading angle and yaw rate achieve stability after 60 s, facilitating reliable circular path tracking. A sudden shift in the heading curve at 300 s arises from the angular constraint within  $[\pi, \pi]$ , a computational adjustment to preserve angle continuity and validity. Regarding velocity regulation, SSL demonstrates competitive stability compared to other methods, with speed stabilization occurring after 60 seconds, ultimately outperforming PPO and ICM-PPO in positional accuracy, heading maintenance, and speed regulation under marine disturbance conditions.

As illustrated in Fig. 9(e), the comparative analysis of

**Table 3**

Error analysis of complex trajectory tracking experiments.

Method	Mean value of $e_x$ after 50 s	Mean value of $e_y$ after 50 s	Mean value of $e$ after 50 s
PPO	1.012m	1.983m	2.432m
ICM-PPO	<b>0.277m</b>	0.566m	0.677m
SSL	0.278m	<b>0.396m</b>	<b>0.537m</b>

trajectory tracking errors reveals that the proposed SSL controller performs better. Upon stabilization within the circular path, SSL exhibits a mean tracking error of 0.218 m, representing a significant reduction of 3.769 m and 0.428 m compared to PPO and ICM-PPO, respectively, as quantitatively detailed in Table 2. This substantial improvement confirms SSL's enhanced tracking precision. Furthermore, the control input analysis in Fig. 9(f) demonstrates that all three methodologies initially reach a maximum propeller revolution of 50 RPS within the first 20 seconds to achieve rapid trajectory convergence. However, the PPO approach displays pronounced instability in revolution control, while both ICM-PPO and SSL exhibit markedly reduced oscillation magnitudes. Notably, SSL demonstrates superior adaptability in dynamically adjusting control inputs in response to environmental disturbances and positional deviations, thereby achieving optimal tracking performance.

### 5.3.3. Complex trajectory

$$L_i = \begin{cases} x_d(t) = w_0(t - t_0) + b_0 \\ y_d(t) = w_1(t - t_0) + b_1 \end{cases} \quad (19)$$

$$A_i = \begin{cases} x_d(t) = a_0 \sin(w_0 + c_0(t - t_0)) + b_0 \\ y_d(t) = a_1 \cos(w_1 + c_1(t - t_0)) + b_1 \end{cases} \quad (20)$$

$$\begin{cases} x_d(t), y_d(t) = L_0, & 0 \leq t < 40 \\ x_d(t), y_d(t) = A_0, & 40 \leq t < 68 \\ x_d(t), y_d(t) = L_1, & 68 \leq t < 107 \\ x_d(t), y_d(t) = A_1, & 107 \leq t < 149 \\ x_d(t), y_d(t) = L_2, & 149 \leq t < 188 \\ x_d(t), y_d(t) = A_2, & 188 \leq t < 206 \\ x_d(t), y_d(t) = L_3, & 206 \leq t < 245 \\ x_d(t), y_d(t) = A_3, & 245 \leq t < 284 \\ x_d(t), y_d(t) = L_4, & 284 \leq t \leq 300 \end{cases} \quad (21)$$

**Table 4**  
Parameters of complex trajectory.

	$a_0$	$w_0$	$c_0$	$b_0$	$a_1$	$w_1$	$c_1$	$b_1$	$t_0$
$L_0$		1.41		200.00	-1.41			300.00	0
$A_0$	-40	-0.79	-0.05	226.87	40	-0.79	-0.05	216.56	39
$L_1$		-1.15		259.55		-1.63		193.50	67
$A_1$	40	-2.19	0.05	247.25	-40	-2.19	0.05	106.70	106
$L_2$		1.99		243.84		-0.17		66.85	148
$A_2$	40	-0.09	0.05	324.97	-40	-0.09	0.05	100.05	187
$L_3$		1.37		354.07		1.45		72.61	205
$A_3$	-40	0.81	-0.05	436.69	40	0.81	-0.05	101.90	244
$L_4$		0.84		472.95		-1.81		118.77	283

In this section, we employ formulas and precise numerical values of parameters to represent the complex trajectory in the experiment conducted by Wu et al. (2024). The trajectory comprises a sequence of linear segments denoted as  $\{L_i\}$  and arcs denoted as  $\{A_i\}$ , which are mathematically represented in Eq. (19) and Eq. (20), respectively. Eq. (21) stipulates the utilization of either linear or arc trajectories across different time intervals  $t(s)$ , with the specific parameter values detailed in Table 4.

In the complex trajectory tracking simulation, the initial conditions were set as follows: the position and heading angle were  $\{x_0 = 185 \text{ m}, y_0 = 330 \text{ m}, \psi_0 = 0.5\pi\}$ , and the initial velocities were  $\{u_0 = 1.128 \text{ m/s}, v_0 = 0 \text{ m/s}, r_0 = 0 \text{ rad/s}\}$ . The control parameters were initialized at  $\eta_0 = 10 \text{ r/s}$  and  $\delta_0 = 0^\circ$ . Environmental factors included a north ( $N, 0^\circ$ ) wind with a speed of  $3 \text{ m/s}$  and a north ( $N, 0^\circ$ ) current with a velocity of  $0.25 \text{ m/s}$ .

Figure Fig. 10 contrasts the simulation outcomes for tracing complex trajectories encompassing arcs and linear segments. An examination of subfigures Fig. 10(a) to Fig. 10(d) reveals that all approaches are competent in adhering

to the reference path under disruptive circumstances. Specifically, Fig. 10(a) demonstrates that PPO experiences varying levels of divergence due to northerly winds and currents, with these deviations intensifying markedly after 110 seconds. Conversely, both ICM-PPO and SSL maintain precise tracking under these conditions. The plot depicting heading changes indicates that between 150 and 250 seconds, substantial heading angle adjustments are made in response to navigating against the northerly wind and current to correct the tracking state. Regarding tracking velocity, the SSL approach exhibits superior stability compared to the other methods. Consequently, our proposed method demonstrates enhanced tracking precision for positional and velocity control, outperforming PPO and ICM-PPO.

As illustrated in Fig. 10(e), the tracking errors of various methodologies are compared. Notably, the SSL approach exhibits a diminished tracking error while maintaining approximate along-track error. Upon transitioning to a straight-line trajectory, the SSL method achieves an average tracking error of  $0.537 \text{ m}$ , which is a reduction of  $1.895 \text{ m}$  compared to the PPO method and  $0.14 \text{ m}$  relative to the ICM-PPO method, underscoring its superior tracking precision, as detailed in Table 3. Analysis of the control input variable curves in Fig. 10(f) reveals that all methods initially reach a propeller revolution peak of  $50 \text{ RPS}$  within the first 30 seconds to rapidly align with the reference trajectory. However, the PPO algorithm demonstrates significant oscillations in revolution control. In contrast, the ICM-PPO and SSL methods exhibit markedly reduced oscillation amplitudes, enabling more effective adjustments of control inputs in response to disturbances and deviations, thereby enhancing tracking efficacy.

### 5.3.4. Time-varying disturbance

The time-varying disturbance experiments were conducted to evaluate the robustness of our proposed SSL trajectory tracking control method under challenging conditions. Considering the inherent limitations of underactuated vessels, such as large time delays, high inertia, input saturation, and underactuation, which typically hinder lateral response and timely adjustments, precise trajectory tracking under strong time-varying disturbances becomes particularly challenging. While most simulation experiments employ static disturbance (Huang et al., 2019; Wu et al., 2024), the dynamic time-varying disturbance conditions can provide a more comprehensive validation of trajectory tracking control algorithms. Therefore, we designed the experiments with time-varying disturbances, randomly generated six distinct disturbance zones on three trajectories (experiments 5.3.1-5.3.3), and conducted simulations without additional model training. As illustrated in Fig. 11 and Table 5, our SSL model demonstrates satisfactory performance despite unpredictable random disturbances, maintaining mean errors within 1 meter (the simulated vessel measures  $7 \text{ m}$  in length and  $1.16 \text{ m}$  in width). Notably, despite the inherent response lag of underactuated vessels, the proposed algorithm can rapidly adapt to sudden lateral disturbance changes and achieve stability, which is

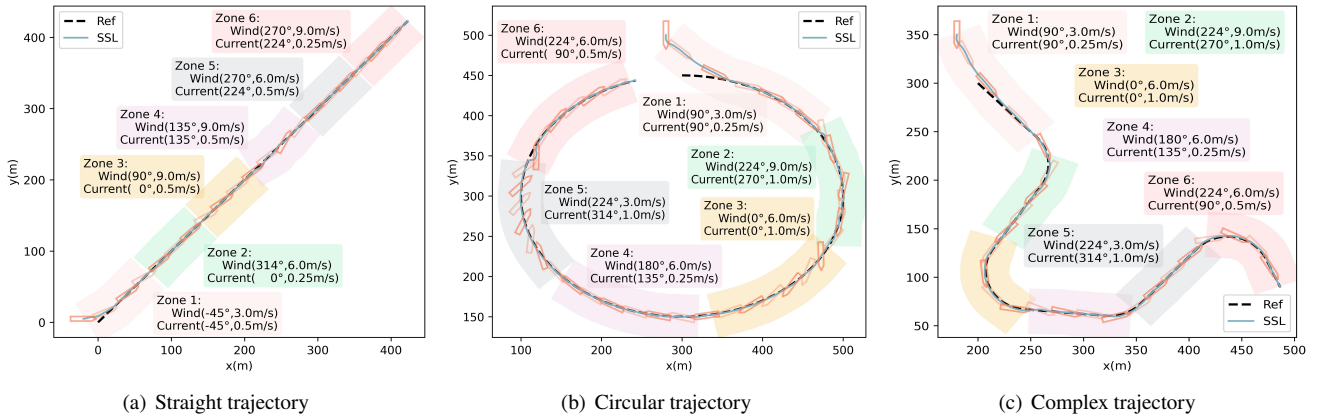


**Fig. 11.** Sailing state with time-varying disturbance.

**Table 5**

Error analysis of time-varying disturbance experiments.

Trajectory	Mean error of different zones (m)												Mean error of whole-zones after 50 s (m)		
	Zone1		Zone2		Zone3		Zone4		Zone5		Zone6		$e_x$	$e_y$	$e$
	$e_x$	$e_y$	$e_x$	$e_y$	$e_x$	$e_y$	$e_x$	$e_y$	$e_x$	$e_y$	$e_x$	$e_y$			
Straight	6.58	3.63	0.07	0.13	0.02	0.15	0.40	0.70	0.02	0.10	0.01	0.04	0.103	0.225	0.269
Circular	10.80	8.71	1.68	0.79	0.24	0.46	0.06	0.18	0.49	0.49	0.84	0.93	0.627	0.532	0.902
Complex	34.94	6.96	0.76	0.41	0.27	0.82	0.12	0.38	0.11	0.23	0.28	0.60	0.306	0.487	0.622

evident in Fig. 11(a) (zones 3-4), Fig. 11(b) (zones 5-6), and Fig. 11(c) (zones 3-4), where the vessel promptly adjusts its heading to maintain stability, thereby validating the robustness of the proposed method. Additionally, while the initial tracking error in zone 1 is relatively large due to the vessel's starting position being distant from the trajectory tracking point, the algorithm effectively reduces the error. Considering the vessel's input saturation, with a maximum speed of approximately 4 m/s in undisturbed conditions and 2 m/s during trajectory tracking tasks, the wind speed was limited to 9 m/s and current speed to 1 m/s, allowing the vessel to maintain maneuverability under disturbances.

## 6. Conclusion

This paper introduces a novel self-supervised learning (SSL) approach for USV trajectory tracking control, addressing high coupling, nonlinear relationships, and environmental disturbances. An innovative adaptive look-ahead distance algorithm is proposed to augment the guidance law, exhibiting exceptional stability even at minimal distances, thus enhancing guidance performance and tracking precision. This stable guidance law underpins a control label generation technique for USV trajectory tracking. The training of controllers has been facilitated through SSL, thereby eliminating the dependency on extensive and labor-intensive manual labeling. Finally, the proposed method has been rigorously tested in various tracking scenarios, including simple and complex trajectories. Simulation results have demonstrated its effectiveness in achieving accurate trajectory tracking control for

USVs. The method improves tracking accuracy and exhibits robustness against the inherent uncertainties and disturbances in the marine environment. Despite these advancements, our SSL approach has certain limitations; specifically, the proposed automatic label generation technique relies on ship parameter tuning, such as the MMG standard method of ship maneuvering predictions, for calculating tracking errors, which may constrain its applicability in scenarios with unknown or highly variable vessel dynamics. Future works include refining the label generation process, simplifying the simulation of arbitrary USVs with a single propeller and rudder, and conducting sea-trial tests to validate performance under real-world conditions, boosting the method's adaptability and further verifying its robustness.

## Acknowledgements

The authors would like to express appreciation for the financial support provided by the National Natural Science Foundation of China (52171308), Natural Science Foundation of Fujian Province (2024J01710), and National Key Research and Development Program of Ministry of Science and Technology (2021YFB3901500).

## References

- Abdulrazzaq, M.M., Ramaha, N.T.A., Hameed, A.A., Salman, M., Yon, D.K., Fitriyani, N.L., Syafrudin, M., Lee, S.W., 2024. Consequential advancements of self-supervised learning (ssl) in deep learning contexts. *MATHEMATICS* 12. doi:10.3390/math12050758.
- Awad, N., Lasheen, A., Elnaggar, M., Kamel, A., 2022. Model predictive control with fuzzy logic switching for path tracking of autonomous vehi-

- cles. *ISA TRANSACTIONS* 129, 193–205. doi:10.1016/j.isatra.2021.12.022.
- Chen, H., Tang, G., Wang, S., Guo, W., Huang, H., 2023. Adaptive fixed-time backstepping control for three-dimensional trajectory tracking of underactuated autonomous underwater vehicles. *OCEAN ENGINEERING* 275. doi:10.1016/j.oceaneng.2023.114109.
- Chu, Y., Wu, Z., Zhu, X., Yue, Y., Lim, E.G., Paoletti, P., 2024. Self-supervised dock pose estimator for unmanned surface vehicles autonomous docking, in: 2024 10th International Conference on Mechatronics and Robotics Engineering (ICMRE), IEEE, pp. 189–194. doi:10.1109/ICMRE60776.2024.10532188.
- Deng, Y., Zhang, X., Im, N., Zhang, G., Zhang, Q., 2020. Adaptive fuzzy tracking control for underactuated surface vessels with unmodeled dynamics and input saturation. *ISA TRANSACTIONS* 103, 52–62. doi:10.1016/j.isatra.2020.04.010.
- Dong, X., Gao, H., Shang, L., 2023. Analysis of key technologies for unmanned surface vessels (usv), in: 2023 2nd International Symposium on Control Engineering and Robotics (ISICER), pp. 158–164. doi:10.1109/ISICER58777.2023.00034.
- Er, M.J., Ma, C., Liu, T., Gong, H., 2023. Intelligent motion control of unmanned surface vehicles: A critical review. *OCEAN ENGINEERING* 280. doi:10.1016/j.oceaneng.2023.114562.
- Fan, Y., Qiu, B., Liu, L., Yang, Y., 2023. Global fixed-time trajectory tracking control of underactuated usv based on fixed-time extended state observer. *ISA TRANSACTIONS* 132, 267–277. doi:10.1016/j.isatra.2022.06.011.
- Ginerica, C., Zaha, M., Gogianu, F., Busoni, L., Trasnea, B., Grigorescu, S., 2021. Observer control: A vision-dynamics learning approach to predictive control in autonomous vehicles. *IEEE ROBOTICS AND AUTOMATION LETTERS* 6, 6915–6922. doi:10.1109/LRA.2021.3096157.
- Gui, J., Chen, T., Zhang, J., Cao, Q., Sun, Z.N., Luo, H., Tao, D.C., 2024. A survey on self-supervised learning: Algorithms, applications, and future trends. *IEEE TRANSACTIONS ON PATTERN ANALYSIS AND MACHINE INTELLIGENCE* 46, 9052–9071. doi:10.1109/TPAMI.2024.3415112.
- Huang, H., Gong, M., Zhuang, Y., Sharma, S., Xu, D., 2019. A new guidance law for trajectory tracking of an underactuated unmanned surface vehicle with parameter perturbations. *OCEAN ENGINEERING* 175, 217–222. doi:10.1016/j.oceaneng.2019.02.042.
- Jia, Z., Hu, Z., Zhang, W., 2019. Adaptive output-feedback control with prescribed performance for trajectory tracking of underactuated surface vessels. *ISA TRANSACTIONS* 95, 18–26. doi:10.1016/j.isatra.2019.04.035.
- Li, Y., Wu, D., Wang, H., Lou, J., 2025. Dynamic collision avoidance for maritime autonomous surface ships based on deep q-network with velocity obstacle method. *OCEAN ENGINEERING* 320. doi:10.1016/j.oceaneng.2025.120335.
- Liang, H., Li, H., Xu, D., 2021. Nonlinear model predictive trajectory tracking control of underactuated marine vehicles: Theory and experiment. *IEEE TRANSACTIONS ON INDUSTRIAL ELECTRONICS* 68, 4238–4248. doi:10.1109/TIE.2020.2987284.
- Liu, H., Qi, Z., Yuan, J., Tian, X., 2023. Robust fixed-time  $h_\infty$  tracking control of uavs with partial and full state constraints and prescribed performance under input saturation. *OCEAN ENGINEERING* 283. doi:10.1016/j.oceaneng.2023.115023.
- Liu, X., Yan, H., Zhou, W., Wang, N., Wang, Y., 2024. Event-triggered optimal tracking control for underactuated surface vessels via neural reinforcement learning. *IEEE TRANSACTIONS ON INDUSTRIAL INFORMATICS* 20, 12837–12847. doi:10.1109/TII.2024.3424573.
- Peng, Z., Wang, D., Wang, J., 2021. Data-driven adaptive disturbance observers for model-free trajectory tracking control of maritime autonomous surface ships. *IEEE TRANSACTIONS ON NEURAL NETWORKS AND LEARNING SYSTEMS* 32, 5584–5594. doi:10.1109/TNNLS.2021.3093330.
- Peng, Z.H., Xia, F.B., Liu, L., Wang, D., Li, T.S., Peng, M., 2024. Online deep learning control of an autonomous surface vehicle using learned dynamics. *IEEE TRANSACTIONS ON INTELLIGENT VEHICLES* 9, 3283–3292. doi:10.1109/TIV.2023.3333437.
- Shin, J., Kwak, D.J., Il Lee, Y., 2017. Adaptive path-following control for an unmanned surface vessel using an identified dynamic model. *IEEE-ASME TRANSACTIONS ON MECHATRONICS* 22, 1143–1153. doi:10.1109/TMECH.2017.2651057.
- Wang, N., Gao, Y., Yang, C., Zhang, X., 2022. Reinforcement learning-based finite-time tracking control of an unknown unmanned surface vehicle with input constraints. *NEUROCOMPUTING* 484, 26–37. doi:10.1016/j.neucom.2021.04.133.
- Wang, N., Gao, Y., Zhao, H., Ahn, C.K., 2021. Reinforcement learning-based optimal tracking control of an unknown unmanned surface vehicle. *IEEE TRANSACTIONS ON NEURAL NETWORKS AND LEARNING SYSTEMS* 32, 3034–3045. doi:10.1109/TNNLS.2020.3009214.
- Wang, Y., Liu, X., Wu, Z., Dang, C., 2024. Distributed prescribed-time formation control for underactuated surface vehicles with input saturation: Theory and experiment. *IEEE TRANSACTIONS ON INTELLIGENT TRANSPORTATION SYSTEMS* 25, 18611–18623. doi:10.1109/TITS.2024.3436882.
- Woo, J., Yu, C., Kim, N., 2019. Deep reinforcement learning-based controller for path following of an unmanned surface vehicle. *OCEAN ENGINEERING* 183, 155–166. doi:10.1016/j.oceaneng.2019.04.099.
- Wu, C., Yu, W., Li, G., Liao, W., 2023. Deep reinforcement learning with dynamic window approach based collision avoidance path planning for maritime autonomous surface ships. *OCEAN ENGINEERING* 284. doi:10.1016/j.oceaneng.2023.115208.
- Wu, C.B., Yu, W.N., Liao, W.Q., Ou, Y.H.C., 2024. Deep reinforcement learning with intrinsic curiosity module based trajectory tracking control for usv. *OCEAN ENGINEERING* 308. doi:10.1016/j.oceaneng.2024.118342.
- Xiaofei, Y., Yilun, S., Wei, L., Hui, Y., Weibo, Z., Zhengrong, X., 2022. Global path planning algorithm based on double dqn for multi-tasks amphibious unmanned surface vehicle. *OCEAN ENGINEERING* 266. doi:10.1016/j.oceaneng.2022.112809.
- Yan, X., Yang, X., Feng, B., Liu, W., Ye, H., Zhu, Z., Shen, H., Xiang, Z., 2024. A navigation accuracy compensation algorithm for low-cost unmanned surface vehicles based on models and event triggers. *CONTROL ENGINEERING PRACTICE* 146. doi:10.1016/j.conengprac.2024.105896.
- Yang, X., She, H., Lou, M., Ye, H., Guan, J., Li, J., Xiang, Z., Shen, H., Zhang, B., 2024. A joint ship detection and waterway segmentation method for environment-aware of usvs in canal waterways. *IEEE TRANSACTIONS ON AUTOMATION SCIENCE AND ENGINEERING* doi:10.1109/TASE.2024.3375300.
- Yang, X.C., Yin, Z.T., Sheng, Y.X., Farina, D., Liu, H.H., 2025. Self-supervised learning for intuitive control of prosthetic hand movements via sonomyography. *IEEE TRANSACTIONS ON CYBERNETICS* 55, 409–420. doi:10.1109/TCYB.2024.3489438.
- Yasukawa, H., Yoshimura, Y., 2015. Introduction of mmg standard method for ship maneuvering predictions. *JOURNAL OF MARINE SCIENCE AND TECHNOLOGY* 20, 37–52. doi:10.1007/s00773-014-0293-y.
- Zhang, C., Wang, C., Wang, J., Li, C., 2020. Neuro-adaptive trajectory tracking control of underactuated autonomous surface vehicles with high-gain observer. *APPLIED OCEAN RESEARCH* 97. doi:10.1016/j.apor.2020.102051.
- Zhang, Q., Pan, W., Reppa, V., 2022. Model-reference reinforcement learning for collision-free tracking control of autonomous surface vehicles. *IEEE TRANSACTIONS ON INTELLIGENT TRANSPORTATION SYSTEMS* 23, 8770–8781. doi:10.1109/TITS.2021.3086033.
- Zhao, B., Zhang, X., Liang, C., Han, X., 2021. An improved model predictive control for path-following of usv based on global course constraint and event-triggered mechanism. *IEEE ACCESS* 9, 79725–79734. doi:10.1109/ACCESS.2021.3084844.
- Zhou, W., Fu, J., Yan, H., Du, X., Wang, Y., Zhou, H., 2023. Event-triggered approximate optimal path-following control for unmanned surface vehicles with state constraints. *IEEE TRANSACTIONS ON NEURAL NETWORKS AND LEARNING SYSTEMS* 34, 104–118. doi:10.1109/TNNLS.2021.3090054.